eNeuro

Research Article: New Research | Neuronal Excitability

Molecular, morphological, and functional characterization of corticotropin-releasing factor receptor 1-expressing neurons in the central nucleus of the amygdala

S. A. Wolfe[1], H. Sidhu[1], R. R. Patel[1], M. Kreifeldt[1], S. R. D'Ambrosio[1], C. Contet[1] and M. Roberto[1]

[1]*Department of Neuroscience, The Scripps Research Institute La Jolla, CA, 92037*

https://doi.org/10.1523/ENEURO.0087-19.2019

Received: 8 March 2019

Revised: 12 May 2019

Accepted: 25 May 2019

Published: 5 June 2019

S.A.W., H.S., R.R.P., M.K., S.D., and C.C. performed research; S.A.W., H.S., R.R.P., C.C., and M.R. analyzed data; S.A.W., R.R.P., and M.R. wrote the paper; C.C. and M.R. designed research; M.R. contributed unpublished reagents/analytic tools.

Funding: HHS | NIH | National Institute on Alcohol Abuse and Alcoholism (NIAAA)
AA021491
AA015566
AA006420
AA017447
AA026685
AA024952
AA026865
AA007456
.

Conflict of Interest: The authors declare no competing financial interests.

W.S.A., S.H., P.R.R., C.C. and R.M. These authors contributed equally

This work was supported by the Pearson Center for Alcoholism and Addiction Research. This work is supported by NIAAA/NIH (AA021491, AA015566, AA006420, AA017447, AA026685, AA024952, F32: AA026865 and T32: AA007456).

Correspondence should be addressed to Marisa Roberto at mroberto@scripps.edu

Cite as: eNeuro 2019; 10.1523/ENEURO.0087-19.2019

Molecular, morphological, and functional characterization of corticotropin-releasing factor receptor 1-expressing neurons in the central nucleus of the amygdala.

Abbreviated title: Phenotyping of CeA CRF_1+ neurons

Wolfe S. A. [#], Sidhu H. [#], Patel R. R. [#], Kreifeldt M., D'Ambrosio S. R., Contet C.* and Roberto M.*[@]

Department of Neuroscience, The Scripps Research Institute La Jolla, CA 92037

[#]These authors contributed equally

* These authors contributed equally

[@]Corresponding author

Author contributions: M.R., C.C. designed research; S.W., H.S., R.P., M.K., S.D. performed experiments; S.W., H.S., R.P., C.C. analyzed data; M.R., S.W., R.P. wrote and edited manuscript; C.C., H.S., M.K. edited manuscript.

Corresponding author: Marisa Roberto mroberto@scripps.edu

Number of pages: 39

Number of figures: 6

Number of tables: 2

Number of words: Abstract: 237, Significance statement: 66, Introduction: 917, Discussion: 1650

Conflict of interest: The authors declare no competing financial interests.

Acknowledgements: This is manuscript number 29813 from The Scripps Research Institute. The authors thank Dr. Nick Justice for providing CRF_1:GFP breeders.

Funding sources: This work was supported by the Pearson Center for Alcoholism and Addiction Research. This work is supported by NIAAA/NIH (AA021491, AA015566, AA006420, AA017447, AA026685, AA024952, F32: AA026865 and T32: AA007456).

ABSTRACT

The central nucleus of the amygdala (CeA) is a brain region implicated in anxiety, stress-related disorders and the reinforcing effects of drugs of abuse. Corticotropin-releasing factor (CRF, *Crh)* acting at cognate type 1 receptors (CRF_1, *Crhr1*) modulates inhibitory and excitatory synaptic transmission in the CeA. Here, we used CRF_1:GFP reporter mice to characterize the morphological, neurochemical and electrophysiological properties of CRF_1 expressing (CRF_1+) and CRF_1 non-expressing (CRF_1-) neurons in the CeA. We assessed these two neuronal populations for distinctions in the expression of GABAergic subpopulation markers and neuropeptides, dendritic spine density and morphology, and excitatory transmission. We observed that CeA CRF_1+ neurons are GABAergic but do not segregate with calbindin, calretinin, parvalbumin, or PKCδ. Among the neuropeptides analyzed, *Penk* and *Sst* had the highest percentage of co-expression with *Crhr1* in both the medial and lateral CeA subdivisions. Additionally, CeA CRF_1+ neurons had a lower density of dendritic spines, which was offset by a higher proportion of mature spines compared to neighboring CRF_1- neurons. Accordingly, there was no difference in basal spontaneous glutamatergic transmission between the two populations. Application of CRF increased overall vescicular glutamate release onto both CRF_1+ and CRF_1- neurons, and does not effect amplitude or kinetics of excitatory post-synaptic currents in either population. These novel data highlight important differences in the neurochemical make-up and morphology of CRF_1+ compared to CRF_1- neurons, which may have important implications for the transduction of CRF signaling in the CeA.

SIGNIFICANCE

Corticotropin-releasing factor (CRF) is involved in emotional regulation via hypothalamic and amygdalar circuits, and is implicated in several psychiatric disorders including anxiety, depression, addiction, posttraumatic stress disorder, and eating disorders. Our novel identification of unique molecular, morphological and functional properties to distinguishing CRF_1+ neurons in the central amygdala represents a critical step in understanding the cellular role and dysregulation of the CRF system in pathological conditions.

INTRODUCTION

The corticotropin-releasing factor (CRF, *Crh*) plays an important role in emotional regulation via hypothalamic and amygdalar circuits under normal physiological conditions (Heilig et al., 1994). Accordingly, dysregulation of the CRF system is implicated in several animal models of psychiatric disorders Despite promising preclinical studies in animal models including anxiety, depression, addiction, posttraumatic stress disorder, and eating disorders (Baiamonte et al., 2014; Bruijnzeel et al., 2012; Chu et al., 2007; Ciocchi et al., 2010; Funk et al., 2007; Iemolo et al., 2013; Ji et al., 2013; Koob, 2003, 2008; Menzaghi et al., 1994; Tye et al., 2011; Valdez et al., 2003). Despite promising preclinical studies in animal models, the clinical studies of CRF_1 antagonists on mood disorders have been unsuccessful (Heilig et al., 2011; Dunlop et al., 2017; Nielsen, 2006; Zorrilla and Koob, 2004). It has been suggested that these differences may be due to several factors including differences between human symptomatology compared to animal behavior, differences in contributions of different CRF_1 populations, or functional state of CRF_1 between humans and animals, and dosage and bioavailability of the CRF_1 antagonists (Kehne and Cain, 2010; Binneman et al., 2008, Cruces et al., 2014; Nielsen, 2006; Zorrilla and Koob, 2004; Dong et al., 2018). Despite these pitfalls, further research is needed to understand more mechanistically the CRF/CRF_1 system which could develop CRF_1 antagonists to be suitable for patient treatment with improved bioavailability and decreased side-effects in humans (Dong et al., 2018; Spierling and Zorrilla, 2017; Pomrenze et al., 2017).

CRF and CRF receptor type 1 (CRF_1, *Crhr1*) expressing neurons are located in several brain regions including the central nucleus of the amygdala (CeA), which

functions as the main output nucleus for amygdala functions (Gilpin et al., 2015). The CeA is comprised of medial (CeM) and lateral (CeL) subdivisions (Davis et al., 2010; Dong et al., 2001; Petrovich et al., 1996; Sun et al., 1991; Ciocchi et al., 2010; McCullough et al., 2018; Haubensak et al., 2010) and contains mostly GABAergic projection neurons and interneurons (Sun and Cassell, 1993; Veinante and Freund-Mercier, 1998). The CeM sends inhibitory projections to various effector regions (e.g., hypothalamus, periaqueductal grey, locus coeruleus, bed nucleus of the stria terminalis (BNST), and pedunculopontine tegmental nucleus) (Pitkanen and Amaral, 1994). The CeL sends inhibitory inputs to CeM, thereby gating the output activity of the CeA, but also to more distant brain regions such as the periaqueductal gray and paraventricular nucleus of the thalamus (Penzo et al., 2014).

Accumulating evidence implicates the CRF/CRF_1 system in the CeA in many animal models of physiological and pathological conditions (Baiamonte et al., 2014; Bruijnzeel et al., 2012; Chu et al., 2007; Funk et al., 2007; Iemolo et al., 2013; Ji et al., 2013; Lowery-Gionta et al., 2012; Roberto et al., 2010). However, cellular heterogeneity in this region has limited the identification and full functional characterization of the CRF_1 expressing (CRF_1+) subset. Thus, we used a bacterial artificial chromosome (BAC) transgenic mouse line expressing the green fluorescent protein (GFP) under the *Crhr1* promoter (CRF_1:GFP) to readily identify neurons expressing CRF_1 (Justice et al., 2008). Previously CRF_1+ neurons were observed to be mainly located in the CeM and exhibit an ongoing tonic GABAergic conductance driven by action potential-dependent GABA release. In contrast, CRF_1 non-expressing (CRF_1-) neurons display no ongoing tonic inhibition (Herman et al., 2013). Although this functional analysis has yielded

115 significant insight into cell type-specific properties in CeA microcircuits, a precise
116 molecular characterization of the CRF_1+ neuronal population is lacking.

117 The expression pattern of several relevant markers in the rat and mouse CeA
118 have been utilized to distinguish neuronal subsets including: calcium-binding proteins
119 (CBPs) (Andressen et al., 1993; Kemppainen and Pitkanen, 2000); neuropeptides such
120 as CRF (Petrovich et al., 1996), somatostatin (*Sst*) (Kim et al., 2017; Li et al., 2013;
121 Penzo et al., 2014; Yu et al., 2016), proenkephalin (PENK, *Penk*) (Poulin et al., 2008),
122 prodynorphin (PDYN, *Pdyn*) (Funk et al., 2006; Merchenthaler et al., 1997; Schwarzer,
123 2009), and neuropeptide Y (NPY, *Npy*) (Gilpin et al., 2015; Lin et al., 2006; McGuire et
124 al., 2011); and Protein Kinase C-δ (PKC-δ, *Prkcd*) (Cai et al., 2014; Haubensak et al.,
125 2010; Herry et al., 2008). However, the patterns of co-expression of these markers with
126 *Crhr1* are unknown.

127 Given the critical role of CRF and CRF_1 in the CeA, we sought to identify unique
128 molecular, morphological and functional properties that distinguish CeA CRF_1+ neurons
129 from their CRF_1- neighbors. Utilizing CRF_1:GFP mice we determined the following
130 characteristics of CeA CRF_1+ and CRF_1- neurons: 1) co-expression patterns of CRF_1
131 (via GFP reporter) with CBPs parvalbumin (PV), calretinin (CR) and calbindin (CB); 2)
132 co-expression patterns of *Crhr1* with *Penk*, *Pdyn*, *Sst*, *Npy*, *Crh*, and *Prkcd*; 3) dendritic
133 spine morphology and density; and 4) basal and CRF-modulated glutamatergic
134 transmission. We found that *Penk* and *Sst* have the highest percentage of co-
135 expression with *Crhr1* in both the CeM and CeL, and that *Penk* is enriched in CeM
136 *Crhr1*+ neurons compared to their *Crhr1*- neighbors. We also show that CeM CRF_1+
137 neurons exhibit an overall lower spine density and differential fractions of mature *versus*

immature spines compared to CRF_1- neurons. Consistent with a comparable density of mature spines in these two populations, we found no difference in spontaneous or miniature excitatory post-synaptic currents. Importantly, acute CRF application increased overall CeM glutamatergic transmission and does not effect amplitude or kinetics of excitatory post-synaptic currents in either population. These data provide important information about the neurobiology of CeA CRF_1+ neurons that may have critical implications for their functional role under physiological and pathological conditions.

MATERIALS AND METHODS

All procedures were approved by our Institutional Animal Care and Use Committee and were consistent with the National Institutes of Health *Guide for the Care and Use of Laboratory Animals.* Transgenic CRF_1:GFP mice were generated on a mixed C57BL/6J x BALB/c background using BAC recombination (see Justice et al., 2008 for transgene design and immunohistochemical validation of reporter expression). A colony was established at our institute in 2008 and has been backcrossed to C57BL/6J mice every 2-3 years since. Mice were genotyped by PCR on tail snip lysates using the following transgene-specific primers: forward 5' GGT CAC CCC AAA AAT AAT CTC T 3'; reverse 5' AGG ATT GGG AAG ACA ATA GC 3'. We also amplified a positive control band using the following primers: forward 5' TCC TCA AAG ATG CTC ATT AG 3'; reverse 5' GTA ACT CAC TCA TGC AAA GT 3'. Adult male mice were used for all experiments.

Immunohistochemistry

Tissue preparation

Mice (n=4) were anesthetized (isoflurane) and perfused with cold phosphate buffered saline (PBS) followed by 4% paraformaldehyde (PFA). Brains were dissected and immersion fixed in PFA for 24 hours at 4°C, cryoprotected in sterile 30% sucrose in PBS for 24-48 hours at 4°C or until brains sank, flash frozen in pre-chilled isopentane on dry ice and stored at -80°C. Free floating 35 µm brain sections were obtained using a cryostat and kept at 4°C in PBS containing 0.01% sodium azide.

Immunohistochemistry

169 Sections were washed in PBS for 10 minutes at room temperature (RT) with
170 gentle agitation and then blocked for 1 hour at RT in blocking solution [0.3% triton X-
171 100, 1mg/ml bovine serum albumin (BSA) and 5% normal goat serum (NGS)]. Primary
172 antibody was incubated at 4^0C overnight with gentle agitation in 0.5% tween-20 and 5%
173 NGS. The following primary antibodies were used: chicken anti-GFP (Abcam, ab13970,
174 RRID:AB 300798; 1:2000), mouse anti-PV (Swant, 235, RRID:AB 10000343; 1:1000),
175 mouse anti-CR (Swant, 6B3, RRID:AB 10000320; 1:500) and mouse anti-CB (Swant,
176 300, RRID:AB 10000347; 1:2000). Next, sections were triple washed in PBS for 10
177 minutes at RT with gentle agitation followed by a 1 hour secondary antibody incubation
178 in PBS (in the dark). The following secondary antibodies were used: Alexa Fluor 488
179 goat anti-chicken (Thermo Fisher Scientific, A-11039, RRID:AB 142924) and Alexa
180 Fluor 568 goat anti-mouse (Thermo Fisher Scientific, A-11004, RRID:AB 141371).
181 Sections were then washed (10 minutes, RT, 3 times) and mounted in Vectashield
182 (Vector labs, H1500, RRID:AB 2336788).

183 *Imaging and analysis*

184 Sections were imaged on a Zeiss LSM 780 laser scanning confocal microscope
185 (10x objective, tile scanning of CeA). All microscope settings were kept the same within
186 experiments during image acquisition. Analyst was blind to the identity of the red
187 fluorescent signal (calcium-binding protein) when performing cell counts, and analysis
188 was performed manually in an unbiased manner at four anterior-posterior levels
189 (equidistant sections located -1.00 through -1.70 mm from bregma). Data are presented
190 as mean ± standard error.

In situ hybridization

Tissue preparation

Mice (n=3-4) were anesthetized (isoflurane) and perfused with cold PBS/Z-fix (Fisher Scientific, NC9378601). Brains were dissected and immersion fixed in Z-fix for 24 hours at 4°C, cryoprotected in sterile 30% sucrose in PBS for 24-48 hours at 4°C or until brains sank, flash frozen in pre-chilled isopentane on dry ice, and stored at -80°C. Brains were then sliced on a cryostat in 20 µm thick sections, mounted on SuperFrost Plus slides (Fisher Scientific, 1255015) and stored at -80°C.

In situ hybridization

In situ hybridization was performed using RNAscope fluorescent multiplex kit (ACD, 320850) in RNase-free conditions. To perform the RNAscope *in situ* hybridization, a target retrieval pretreatment protocol was performed as outlined in the manual (ACD, doc.no. 320535). Briefly, slides were submersed in target retrieval buffer (ACD, 322000) at 95-98°C for 10 minutes, immediately washed in distilled water, dehydrated with 100% ethanol (storage at -80°C if required), and lastly digested with Protease IV for 20 min at 40°C. Following this pretreatment the RNAScope Fluorescent Multiplex Reagent Kit User Manual (ACD, doc.no. 320293) was followed and slides were mounted with DAPI-containing Vectashield (Fisher Scientific, NC9029229). A negative control (ACD, 320751) was run in tandem for each experiment. The probes used from ACD Biotechne were as follows: *Crhr1* (418011-C1, -C2), *Gad2* (439371-C3), *Slc17a7* (416631-C2), *Penk* (318761), *Pdyn* (318771), *Sst* (404631), *Npy* (313321), *Prkcd* (441791), *Crh* (316091), and eGFP (400281).

Imaging and analysis

Slides were imaged on a Zeiss LSM 780 laser scanning confocal microscope (40X oil immersion, 1024x1024, tile scanning of CeA at approximately bregma -1.46mm, 5-µm z-stacks). All microscope settings were kept the same within experiments during image acquisition. To perform quantification, ImageJ (Schindelin et al., 2012) was used to outline individual nuclei as identified by DAPI staining and count all nuclei in an unbiased manner (all settings kept the same within experiments). The fluorescence intensity for each probe per DAPI counted nuclei was then measured and the background signal, as determined by the average intensity of the negative control, was subtracted for each channel. For each probe, signal intensity present after background subtraction identified positive nuclei. Experiment was performed in an unbiased manner as probe fluorescence was quantified blindly, independently, and after nuclei identification by computational means.

Next, the percentage of nuclei positive for one or both probes and the percent of signal co-expression were calculated. Percent of total nuclei was determined by dividing the total number of nuclei expressing that marker by the total number of DAPI positive nuclei per image. The percent of *Crhr1*+ nuclei expressing a marker of interest was determined by dividing the number of co-labeled nuclei by the total number of *Crhr1*+ nuclei. The percent of *Crhr1*- nuclei co-expressing a marker of interest was determined by dividing the number of cells expressing the marker of interest but not *Crhr1* by the total number of *Crhr1*- nuclei per image. *Crhr1*+ compared to *Crhr1*- patterns of co-expression was assessed and normalized to the *Crhr1*- cells.

For densitometry, signal intensity measured after background subtraction was quantified, log2 transformed, and normalized to the CeL for visualization of the difference in expression. Unpaired Student's t-test was used to assess significance of the CeL vs. CeM expression difference for each gene, as well as the *Crhr1*+ to *Crhr1*- percent co-expression of each gene. Analysis and statistics were performed using R programming (R Core Team, 2018). All analyses were performed on raw images. Outliers detected by Grubb's test. Brightness/contrast and pixel dilation are the same for all representative images shown per figures.

Dendritic spine analysis

Tissue preparation

Mice (n=4) were anesthetized (isoflurane) and perfused with cold PBS/4% PFA. Brains were extracted and immersion fixed in 4% PFA at 4°C for 2 hours before being sectioned coronally into 100 µm slices on a vibrating microtome (Leica VT1000S, Leica Microsystems).

Biolistic labeling

Sections were biolistically labeled with DiI (1,1′-dioctadecyl-3,3,3′,3′-tetramethylindocarbocyanine perchlorate) coated 1.1 µm tungsten particles delivered with a BioRad gene gun and incubated in PBS overnight at 4°C before immunostaining. Slices were permeabilized in 0.01% triton X-100 for 15 minutes at RT with gentle agitation and blocked for 30 minutes at RT with gentle agitation in blocking solution (10% NGS in 0.01% triton X-100). Primary antibody incubation was performed overnight

256 at 4^{0}C in PBS (chicken anti-GFP; Abcam, ab13970, RRID:AB 300798; 1:2000). The
257 slices were triple washed with PBS for 10 minutes followed by secondary antibody
258 incubation for 1 hour at RT in blocking solution (Alexa Fluor 488 goat anti-chicken;
259 Thermo Fisher Scientific, A-11039, RRID:AB 142924). The slices were triple washed in
260 PBS and mounted on slides with Prolong Diamond (Thermo Fisher Scientific, P36965).

261 *Imaging and analysis*

262 Slides were imaged for CeA on a Zeiss LSM 710 laser scanning confocal
263 microscope (Carl Zeiss MicroImaging; 63x oil immersion, 1024x1024, 1 µm step z-
264 stacks). All microscope settings were kept the same within experiments during image
265 acquisition. ImageJ (Schindelin et al., 2012) was used to perform a quantification of
266 filopodia, thin, stubby and mushroom-shaped dendritic spines in both CRF_1+ (n=13
267 neurons, 37 dendritic segments) and CRF_1- neurons (n=29 neurons, 41 dendritic
268 segments). The experimenter was blind to cell type (CRF_1+ *vs* CRF_1-) when performing
269 spine quantification. Data obtained in each mouse were averaged for each cell type,
270 such that the number of mice was used as the n in statistical analyses. Spine densities
271 and spine type proportions in CRF_1- and CRF_1+ neurons were compared using paired t-
272 tests. Data are presented as mean ± standard error. In all cases, $p<0.05$ was the
273 criterion for statistical significance.

274 ***Electrophysiological recordings***

275 *Brain slice preparation*

Mice (n=12) were briefly anesthetized with 3-5% isoflurane and decapitated. Brains were rapidly removed and placed in an ice-cold high-sucrose solution (pH 7.3-7.4) that contained (in mM): sucrose 206.0; KCl 2.5; $CaCl_2$ 2.5; $MgCl_2$ 7; NaH_2PO_4 1.2; $NaHCO_3$ 26; glucose 5; HEPES 5. Brains were cut into coronal sections (300 µm) using a Leica 1200s vibratome (Leica Microsystems, Buffalo Grove, IL) and placed in oxygenated (95% O_2/5% CO_2) artificial cerebrospinal fluid (aCSF) solution composed of the following (in mM): NaCl 130; KCl 3.5; $CaCl_2$ 2; NaH_2PO_4 1.25; $NaHCO_3$ 24; Glucose 10. Slices were incubated in aCSF for 30 minutes at 37°C, followed by a minimum 30 minutes equilibration at RT (21–22°C) before use.

Electrophysiological recordings

We visualized neurons using infrared differential interference contrast (IR-DIC) optics and CCD camera (Infinity 3 s, Lumenera). A 60x magnification water immersion objective (Olympus) was used for identifying and approaching neurons. To avoid photolytic damage, initial exposure to episcopic fluorescence illumination was brief (<2 s). We detected fluorescent neurons using the Lumen 300 LED system (Prior Scientific, UK) and captured images using Luminera software (Lumenera Corp., Ottawa, ON). Whole-cell current-clamp and voltage-clamp recordings were obtained with patch pipettes (3-4 MΩ; Warner Instruments) using a Multiclamp 700B amplifier (Molecular Devices, Sunnyvale, CA), sampled at 20 kHz, low pass filtered at 10 kHz, digitized (Digidata 1440A; Axon Instruments), and stored on a computer using pClamp 10 software (Axon Instruments). Series resistance was not compensated but monitored throughout the experiment, and cells with a series resistance >15MΩ or a >20% change were excluded.

The intracellular solution used for voltage and current clamp recordings was composed of (in mM): potassium gluconate 145; EGTA 0.5; $MgCl_2$ 2; HEPES 10; Na-ATP 2; Na-GTP 0.2. Drugs were dissolved in aCSF and applied by bath perfusion. To isolate spontaneous and miniature excitatory postsynaptic currents (sEPSCs and mEPSCs), recordings were performed in the presence of $GABA_A$ (30 μM bicuculline) and $GABA_B$ (1 μM CGP 55845A) receptor antagonists, and tetrodotoxin (TTX; 0.5 μM) was included for mEPSCs. CeA neurons were held at -60 mV for voltage-clamp recordings and maintained at -70 mV for current-clamp recordings.

Drugs and chemicals

We purchased CGP 55845A (1 μM) and CRF (200 nM) from Tocris Bioscience, bicuculline methiodide (30 μM) and TTX (0.5 μM) from Sigma.

Statistical analysis

Frequency, amplitude, rise and decay time of EPSCs were analyzed and visually confirmed using a semi-automated threshold based mini detection software (Mini Analysis, Synaptosoft Inc.). Average EPSC characteristics were determined during baseline and experimental drug conditions in 3 minute bins containing a minimum of 60 events. All detected events were used for event frequency analysis, but superimposed events were eliminated for amplitude and kinetic analysis. Data are presented as mean ± standard error, and statistical significance was assessed using a two-tailed t-test or one-sample t-test using Prism 6 (Graphpad Prism). In all cases, $p<0.05$ was the criterion for statistical significance, and *n* represents the number of cells or mice as indicated.

RESULTS

Expression of calcium binding proteins in CeA CRF_1+ neurons

The calcium-binding proteins (CBPs) CB, CR and PV label distinct subsets of neurons in the brain and have been widely used as markers of neuronal populations in the amygdala (Andressen et al., 1993; Kemppainen and Pitkanen, 2000). We therefore examined the expression profile of CBPs in CeA GFP+/CRF_1+ neurons (**Fig. 1**). Using immunohistochemistry in CRF_1:GFP mouse brain sections, the co-expression of PV (PV, **Fig. 1A**), CR (**Fig. 1B**), and CB (**Fig. 1C-D**) with GFP was analyzed in the CeA. Of the CBPs labeled, CB was the most widely expressed, while CR was expressed in few cells and PV was virtually absent from the CeA (**Fig. 1E**). The majority of CeA GFP+ cells were located in the CeM, as described previously (Justice et al., 2008; Herman et al., 2013). The percentage of CRF_1+ cells co-expressing each CBP followed the same pattern as the overall counts of CBP+ cells, wherein CB was present in 19%, CR was present in 2%, and PV was present in 0.1% of CRF_1+ cells (**Fig. 1F**). Based on GFP labeling in CBP+ cells, CRF_1 was present in 58% of CB+ cells and 63% of CR+ cells, and no PV+ cells (**Fig. 1G**).

Expression of neuropeptides and subpopulation markers in CeA Crhr1+ neurons

We next examined the expression of subpopulation markers, including neuropeptides, in *Crhr1*+ neurons in both the CeL and CeM (**Fig. 2A**). We utilized RNAscope multiplex fluorescent *in situ* hybridization technology to detect single RNA transcripts. First, the validity of the CRF_1:GFP transgenic mice was assessed through

the co-expression of GFP mRNA and *Crhr1* mRNA in the CeL and CeM where 58% and 86% co-expression was observed respectively. (**Fig. 2B**), and the *Crhr1* probe was validated in the septum, a region of low CRF_1 expression(Van Pett et al., 2000) (**Fig. 2C**). Glutamic acid decarboxylase 2 (*Gad2*) and vesicular glutamate transporter 1 (*Slc17a7*) were used as GABAergic and glutamatergic neuronal markers, respectively. *In situ* hybridization in both the CeL (**Fig. 2D-F**) and CeM (**Fig. 2G-I**) identified a high proportion of nuclei expressing *Gad2*, 89% and 98% respectively, and a low proportion expressing *Slc17a7*, 3% and 4% respectively. This is consistent with the majority of neurons being GABAergic in this region (Ehrlich et al., 2009; Pitkanen and Amaral, 1994). Almost all *Crhr1*+ cells expressed *Gad2* at 98% in the CeL and 100% in the CeM (**Fig. 2E,H**), whereas very few expressed *Slc17a7* at 6% in the CeL and 5% in the CeM (**Fig. 2F,I**). Additionally, a negative control was run in each series for background subtraction (**Fig. 2J**). *Crhr1* expression was observed in about 23% and 34% of all nuclei on average in CeL and CeM, respectively. These data indicate that CeA *Crhr1*+ neurons, as well as the vast majority of CeA neurons, are GABAergic and are located in both the CeL and CeM.

Co-expression of *Crhr1* with the neuropeptides *Penk*, *Sst*, *Pdyn*, *Crh*, and *Npy,* as well as with *Prkcd*, was also examined (CeL **Fig. 3A-F**; CeM, **Fig. 4A-F**). In the CeL, transcripts for all these genes, except *Npy*, were found in high abundance, where *Penk* was expressed in 86% of cells, *Sst* in 59%, *Pdyn* in 58%, *Prkcd* in 71%, *Crh* in 36%, and *Npy* in 5% of cells (**Fig. 3G**). The proportion of total nuclei expressing each of these transcripts was similar to the proportion observed in *Crhr1*+ nuclei only, where *Penk* was expressed in 92%, *Sst* in 75%, *Pdyn* in 70%, *Prkcd* in 53%, *Crh* in 42%, and *Npy* in

10% of *Crhr1*+ cells (**Fig. 3H**). Accordingly, when comparing the expression of the above peptides in CeL *Crhr1*+ vs. *Crhr*1- neurons no significant differences were observed between the two populations (**Fig. 3I**).

The CeM showed a similar general co-expression pattern as the CeL (**Fig. 4A-F**). However, the proportion of total nuclei expressing neuropeptides was overall lower, with the percent expressing *Penk* at 42%, *Sst* at 26%, *Crh* at 18%, *Pdyn* at 15%, *Prkcd* at 11%, and *Npy* at 7% (**Fig. 4G**). Similar proportions were observed in *Crhr1*+ nuclei only, with the percent expressing *Penk* at 65%, *Sst* at 42%, *Crh* at 27%, *Pdyn* at 23%, *Prkcd* at 7%, and *Npy* at 10% (**Fig. 4H**). *Penk* and *Sst* again presented the strongest co-expression and *Npy* the weakest. When comparing the expression of the above peptides in CeM *Crhr1*+ vs. *Crhr1*- neurons, *Penk* was found significantly enriched in *Crhr1*+ neurons (1.9 fold, p=0.004; **Fig. 4I**). Lastly we compared the density of nuclear expression of these co-expressed genes in CeM compared to CeL *Crhr1*+ nuclei (**Fig. 4J**), and found that the CeM expressed significantly lower amounts of RNA for all targets [*Crh* (-1.2 fold, p=1.2e-7), *Prkcd* (-1.84 fold, p=1.3e-14), *Pdyn* (-2.3 fold, p=8.4e-11), and *Sst* (-2.95 fold, p=3.8e-10)] except *Penk,* which was expressed at equivalent levels in CeM and CeL (-0.07 fold), and *Npy* (2.7 fold, p=2.5e-7), whose mRNA density was higher in CeM. Additionally, we observed that *Crhr1* density was higher in the CeM compared to the CeL (p=2.2e-16) (**Fig. 4J**).

Dendritic spine morphology and density in CRF_1+ and CRF_1- CeM neurons

Higher levels of GFP and *Crhr1* mRNA expression were observed in the CeM than in the CeL (**Figs. 1-4**), as previously reported (Justice et al., 2008; Herman et al., 2013). We therefore focused subsequent analyses of CRF_1+ and CRF_1- neurons in the CeM. We first analyzed dendritic spines using biolistic labeling of neurons with a lipophilic fluorescent dye followed by GFP immunostaining (**Fig. 5A-B**). Spine density in CRF_1+ (11 spines/10 µm) neurons was lower than in CRF_1- (16 spines/10 µm) neurons (**Fig. 5C**, paired t-test, t_3=-3.3, $p<0.05$). We further analyzed the morphology of dendritic protrusions and calculated the proportion of mushroom spines, stubby spines, thin spines and filopodia in CRF_1+ (49%, 24%, 27%, and 0.7%, respectively) and CRF_1- neurons (41%, 23%, 34%, and 1.2%, respectively) (**Fig. 5D**). The proportion of mushroom spines was significantly higher (t_3=4.9, $p<0.05$) while the proportion of thin spines was significantly lower (t_3=-4.9, $p<0.05$) in CRF_1+ neurons compared to CRF_1- neurons. There were no differences in the proportion of stubby spines (t_3=0.4, n.s.) and filopodia (t_3=-1.0, n.s.) between the two cell types.

Glutamatergic transmission in CRF_1+ and CRF_1- neurons in the CeM

We next examined glutamatergic transmission in CRF_1+ and CRF_1- CeM neurons. Prior to recording glutamatergic activity, whole-cell current clamp recordings with a step protocol consisting of hyperpolarizing to depolarizing current injections were obtained from each cell to determine cell type based on spiking characteristics. As previously described, CeA neurons are composed of three principal cell types: regular spiking, low threshold bursting, and late spiking neurons (Chieng et al., 2006; Dumont et al., 2002; Herman et al., 2013) (**Fig. 6A**). CRF_1+ neurons consisted of only regular

411 spiking and low threshold bursting cell-types as previously reported (Herman et al.,
412 2013, 2016), while the majority of CRF_1- neurons were regular spiking and late spiking
413 neurons (**Fig. 6B**). No significant differences were observed in the membrane properties
414 of CRF_1+ and CRF_1- CeA neurons (**Table 1**).

415 We then assessed baseline glutamatergic transmission using whole-cell voltage
416 clamp recordings of spontaneous action-potential dependent and miniature action-
417 potential independent excitatory postsynaptic currents (sEPSCs and mEPSCs,
418 respectively) in CRF_1+ and CRF_1- CeM neurons (**Fig. 6C-H**). We observed similar
419 baseline mEPSC frequency ($t(26) = 1.3$, n.s.) and amplitude ($t(26) = 1.23$, n.s.) in
420 CRF_1+ (0.9 ± 0.16 Hz; 30.6 ± 1.4 pA; $n = 16$) and CRF_1- neurons (1.6 ± 0.5 Hz; 28.0 ±
421 1.4 pA; $n = 12$) (**Fig. 6 C-E**), and there were no differences in rise and decay kinetics of
422 mEPSCs (**Table 2**). We also observed similar baseline sEPSC frequency ($t(26) = 0.75$,
423 n.s.) and amplitude ($t(26) = 0.70$, n.s.) in CRF_1+ (1.3 ± 0.3 Hz; 28.9 ± 0.8 pA; $n = 14$)
424 and CRF_1- neurons (1.0 ± 0.2 Hz; 28.1 ± 0.6 pA; $n = 14$) (**Fig. 6 F-H**), and there were no
425 differences in rise and decay kinetics of sEPSCs (**Table 2**). Overall, these two
426 populations receive similar glutamatergic input, consistent with their similar density of
427 mature spines.

428

429 ***CRF effects on glutamatergic signaling in CRF_1+ and CRF_1- CeM neurons***

430 To assess differences in the functional responsivity of CRF_1+ and CRF_1-
431 populations to CRF, we tested the effect of CRF (200 nM; 9-12 min) on mEPSCs (**Fig.**
432 **6I-N**). We found that CRF application increased mEPSC frequency in both CRF_1+ ($t(10)$
433 $= 2.78$, $p<0.05$) and CRF_1- ($t(8) = 2.68$, $p<0.05$) CeM neurons (**Fig. 6J**) but did not

434 significantly alter mEPSC amplitude, (CRF_1+: t(10) = 0.50, n.s.; CRF1-:t(8) = 1.12, n.s.,
435 **Fig. 6K**), rise time (CRF_1+: t(10) = 1.28, n.s.; CRF1-:t(8) = 0.95, n.s., **Fig. 6M**), and
436 decay time (CRF1+: t(10) = 1.32, n.s.; CRF1-: t(8) = 0.85, n.s., **Fig. 6N**) of mEPSCs in
437 either population (**Fig. 6**). In summary, CRF globally increases glutamatergic
438 transmission in the CeM via increased presynaptic GABA release, but does not alter
439 mEPSC amplitude or kinetics, suggesting a lack of postsynaptic effect of CRF in either
440 population.

441

442 **DISCUSSION**

443

444 Here we investigated the neurochemistry, morphology, and physiology of CRF_1+
445 neurons in the CeA of adult male mice. We found that calbindin is the predominant CBP
446 expressed in the CeA but overall there is no specific enrichment or exclusion of CBPs in
447 *Crhr1*+ neurons. Co-expression analysis using *in situ* hybridization revealed *Crhr1* co-
448 expressed mostly with *Penk* and *Sst* and least with *Npy*. In the CeM, *Penk* is
449 significantly enriched in CRF_1+ neurons compared to CRF_1- neurons. Morphologically,
450 CRF_1+ neurons have a lower spine density compared to CRF_1- neurons. This difference
451 selectively affects thin spines, while the proportion of mushroom and stubby spines are
452 similar in the two populations. Accordingly, basal excitatory transmission between
453 CRF_1+ and CRF_1- neurons are similar. Additionally, acute CRF application increases
454 glutamatergic transmission in both CRF_1+ and CRF_1- neurons, but induces post-
455 synaptic increases in sEPSC kinetics selectively in CRF_1+ neurons. While there are
456 clear functionally important differences of the CRF_1+ population, revealed by the CRF-

induced sEPSC effects we observed, the lack of enrichment or exclusion of any particular CBP or neuropeptide in this population contributes to the difficulty in identifying and studying this subpopulation in this heterogenous region.

Calcium binding protein and neuropeptide expression in the CRF_1+ subpopulation

GABAergic interneurons may be subcategorized based on their expression of the CBPs PV, CB and CR, and these distinct subpopulations exhibit unique differences in their physiology, synaptology, and morphology (Kemppainen and Pitkanen, 2000). We found that CB was the predominant CBP in both CeL and CeM nuclei, with only a limited number of neurons expressing PV and CR. This pattern of relative CBP expression is in general agreement with immunohistochemical studies conducted in the rat (Kemppainen and Pitkanen, 2000), and with our previous finding that at least 30% of CeA CRF_1-expressing neurons project out to the dorsolateral BNST (Herman et al., 2013, 2016) – one of several downstream brain regions innervated by the CeA.

In addition, CeA neurons can express several neuropeptides that play important roles in fear and anxiety behaviors such as CRF, enkephalins, dynorphins, somatostatin and neuropeptide Y. The overlapping expression pattern of these neuropeptides differentiates distinct neuronal subpopulations in several brain regions in mice and rats (Cai et al., 2014; Haubensak et al., 2010; Herry et al., 2008; Kim et al., 2017; Li et al., 2013; Penzo et al., 2014; Petrovich et al., 1996; Yu et al., 2016). We hypothesized that CRF_1 expression is restricted to a subset of CeA neurons that co-express a unique combination of neuropeptides. Most of the neuropeptides we investigated had similar

trends in the total population compared to the *Crhr1*+ population. However, *Penk* was present in a higher proportion of *Crhr1*+ cells than *Crhr1*- cells in the CeM. *Npy* also trended towards an enrichment in *Crhr1*+ cells over *Crhr1*- cells in the CeL but co-expression results obtained for this neuropeptide showed more variability than for other markers, most likely due to the small number of *Npy*+ nuclei. Additionally, densitometry identified a higher expression of *Crh*, *Pdyn*, *Prkcd*, and *Sst* in the CeL compared to the CeM, which is in agreement with previous studies in mice and rats (Kim et al., 2017; Li et al., 2013; Marchant et al., 2007; McCullough et al., 2018; Veinante et al., 1997; Day et al., 1999). Conversely, *Npy* was present at higher levels in the CeM than in the CeL.

The enrichment of *Penk* in CeM *Crhr1*+ neurons compared to their *Crhr1*- neighbors may have functional relevance for the recruitment of CeA *Penk*+ neurons in response to food, drugs and stress. CeA *Penk*+ are activated by subchronic exposure to fat, ethanol, and nicotine, as well as by withdrawal from morphine in animal models (Chang et al., 2014; Criado and Morales, 2000; Loughlin et al., 2006; Veinante et al., 2003). This activation of CeA *Penk*+ neurons may result from their preferential expression of CRF_1 as some of these stimuli are known to increase CRF_1 signaling in the CeA (Nie 2004, Henrichs 1995). Furthermore, chemogenetic activation of CeA *Penk* neurons produces sustained analgesia, suggesting that CRF_1-mediated activation of these neurons could mediate stress-induced analgesia (Paretkar and Dimitrov, 2019; Wiedenmayer et al., 2002).

It is important to consider here that our method for identification of expressing cells is semi-quantitative and that only signal co-expressing with DAPI staining after stringent background subtraction was quantified to increase confidence in detection.

However, by excluding cell bodies and processes, we lost data concerning dynamic somatic and neurite expression. This method is also limited in its ability to destinguish only neuronal cells which may introduce a consitent level of non-neuronal cells in our analysis. Additionally, co-expression may vary from the rostral to caudal CeA, and a more in-depth study of CeA neuropeptide localization is necessary to identify the role of these neuropeptides in the CRF_1+ subpopulation throughout the CeA. Further studies to identify dynamic expression for RNA or protein at subcellular levels may yield additional information concerning the functional roles of these peptides and proteins.

Our *in situ* hybridization analysis of *Crhr1* expression may yield differing results than GFP expression in the CRF_1:GFP mice due to differences in RNA vs. protein expression, sensitivity of the methods used, image acquisition, and identification of GFP saturated soma vs. puncta quantification in DAPI-stained nuclei. However, the *Crhr1* probe was verified to yield negligible signal in the septum, a region with no CRF_1/GFP expression (Van Pett et al., 2000). Furthermore, our observation that *Crhr1* mRNA density is markedly higher in the CeM than in the CeL is consistent with the patterns of GFP native fluorescence and immunohistochemical staining reported here (**Fig. 2B**) and previously (Justice et al., 2008; Herman et al., 2013), with GFP expression being substantially more prominent in the CeM than in the CeL. This is reflected in the analysis of *Crhr1* vs. GFP mRNA co-expressing cells. A strong co-expression was found between *Crhr1* and GFP mRNA in the CeL and CeM however this was considerably higher in the CeM (**Fig. 2B**). The higher sensitivity of the RNAscope assay compared to native fluorescence and immunohistochemistry probably explains why

about 23% CeL cells are detected as *Crhr1*+, while a very limited number of CeL cells are identified as GFP+."

CRF_1+ neurons differ from CRF_1- neurons in their dendritic morphology

We characterized the dendritic morphology of CeA CRF_1+ and CRF- neurons including spine density and spine shape. The morphology and density of spines plays a crucial role in synaptic and neuronal function. More mature and enlarged spines (mushroom/stubby) are associated with increased synaptic strength, whereas immature spines (thin/filopodia) may sustain limited synaptic signaling (De Roo et al., 2008) Sala and Segal, 2014). Abnormalities in spine morphology are associated with a variety of neurological and psychiatric disorders, including addiction (Varodayan et al., 2018; Herms and Dorostkar, 2016; Mulholland and Chandler, 2007; Phillips and Pozzo-Miller, 2015; Qiao et al., 2016; Spiga et al., 2014). Previous morphological characterization of CeA neurons has identified different cell types (Chieng et al., 2006; McDonald, 1982). Most neurons in the CeM have long dendrites that branch sparingly and have a moderate number of dendritic spines, while a smaller number of neurons have thick dendrites with virtually no spines (McDonald, 1982). Here we observed that the spine density in CRF_1+ neurons was lower than in CRF_1- neurons. We further analyzed the spine type proportions in CRF_1+ and CRF_1- neurons and found a higher proportion of mushroom spines and lower proportion of thin spines in CRF_1+ neurons. The lower overall spine density is therefore at least partially offset by a higher fraction of mushroom (i.e., most mature) spines, resulting in a comparable density of functional spines in CRF_1+ and CRF_1- neurons.

CRF modulation of glutamatergic transmission in CRF_1+ vs. CRF_1- neurons

CRF modulates glutamate transmission and has been shown to increase vesicular glutamate release at rat CeA synapses, which can be enhanced by CRF_1 activity (Varodayan et al., 2017). Therefore, we examined glutamatergic transmission in CRF_1+ and CRF_1- cells as well as the effect of CRF on glutamatergic transmission in these neuronal populations. Both populations receive similar glutamatergic input, consistent with the similar density of functional spines in CRF_1+ and CRF_1- neurons. Additionally, CRF increases mEPSC frequency in both populations with no effect on mEPSC amplitude or kinetics in either population. These results are indicative of CRF-induced increased presynaptic GABA release with no postsynaptic effect on glutamatergic receptors.

Conclusion

Our results reveal molecular, morphological and functional characteristics of CRF_1+ neurons highlighting the importance of identifying specific cell populations in the CeA. The CeA is a hub that integrates disparate inputs (stress) and drives appropriate behavioral outputs. Previous work has demonstrated a major role of the CRF system, and particularly the CRF_1 receptors, within the amygdala complex to influence cellular functions that produce maladaptive behavior in animal models. The amygdalar CRF_1 system represents a common pathway for the convergence of stress, addiction, pain, depression, memory formation and anxiety-related signaling (Koob 2008; Koob 2003, Zorrilla and Koob 2004). In particular, CRF_1 mechanisms and circuits have been

implicated in the development of the negative emotional state associated with alcohol dependence, and it has been proposed that alleviation of this negative state drives the motivation to drink in mice and rats (Koob, 2010; Funk et al., 2006; Roberto et al., 2010; Lowery-Gionta et al., 2012). Our cellular studies revealed that acute and chronic alcohol induced significant alterations in GABAergic signaling in the CeA circuitry. In addition, this GABAergic signaling is cell type-specific for the CRF_1+ subpopulation and their connectivity and may contribute to the development of alcohol dependence (Herman et al., 2016).

Our new evidence on the CRF_1+ cellular phenotype detail the distinct neuronal CeA subpopulations in normal amygdalar function and highlights the need for their further characterization (including intracellular signaling etc) under pathological conditions, such as alcohol dependence and anxiety disorders. The multiplicity of neuronal subpopulations and the complexity of local microcircuits provide numerous targets for potential dysregulation by drugs of abuse (e.g. alcohol) and stress, and their potential clinical relevance.

References

Andressen C, Blumcke I, Celio MR (1993) Calcium-binding proteins: selective markers of nerve cells. Cell Tissue Res 271:181-208.

Baiamonte BA, Valenza M, Roltsch EA, Whitaker AM, Baynes BB, Sabino V, Gilpin N W (2014) Nicotine dependence produces hyperalgesia: role of corticotropin-releasing factor-1 receptors (CRF1Rs) in the central amygdala (CeA). Neuropharmacology 77:217-223.

Binneman B, Feltner D, Kolluri S, Shi Y, Qiu R, Stiger T (2008) A 6-week randomized, placebo-controlled trial of CP-316,311 (a selective CRH1 antagonist) in the treatment of major depression. Am J Psychiatry 165(5):617-620

Bruijnzeel AW, Ford J, Rogers JA, Scheick S, Ji Y, Bishnoi M, Alexander JC (2012) Blockade of CRF1 receptors in the central nucleus of the amygdala attenuates the dysphoria associated with nicotine withdrawal in rats. Pharmacol Biochem Behav 101:62-68.

Cai H, Haubensak W, Anthony TE, Anderson DJ (2014) Central amygdala PKC-delta(+) neurons mediate the influence of multiple anorexigenic signals. Nat Neurosci 17:1240-1248.

Chang GQ, Karatayev O, Barson JR, Liang SC, Leibowitz SF (2014) Common effects of fat, ethanol, and nicotine on enkephalin in discrete areas of the brain. Neuroscience 277:665-678.

Chieng BC, Christie MJ, Osborne PB (2006) Characterization of neurons in the rat central nucleus of the amygdala: cellular physiology, morphology, and opioid sensitivity. J Comp Neurol 497:910-927.

Chu K, Koob GF, Cole M, Zorrilla EP, Roberts AJ (2007) Dependence-induced increases in ethanol self-administration in mice are blocked by the CRF1 receptor antagonist antalarmin and by CRF1 receptor knockout. Pharmacol Biochem Behav 86:813-821.

Ciocchi S, Herry C, Grenier F, Wolff SB, Letzkus JJ, Vlachos I, Ehrlich I, Sprengel R, Deisseroth K, Stadler MB, Muller C, Luthi A (2010) Encoding of conditioned fear in central amygdala inhibitory circuits. Nature 468:277-282.

Criado JR, Morales M (2000) Acute ethanol induction of c-Fos immunoreactivity in pre-pro-enkephalin expressing neurons of the central nucleus of the amygdala. Brain Res 861:173-177.

630 Cruces J, Venero C, Pereda-Perez I, De la Fuente M (2014) A higerh anxiety state in
631 old rats after social isolation is associated to an impairment of the immune response. J
632 Neuroimmunology 277:18-25.
633
634 Davis M, Walker DL, Miles L, Grillon C (2010) Phasic vs sustained fear in rats and
635 humans: role of the extended amygdala in fear vs anxiety. Neuropsychopharmacology
636 35:105-135.
637
638 De Roo M, Klauser P, Garcia PM, Poglia L, Muller D (2008) Spine dynamics and
639 synapse remodeling during LTP and memory processes. Prog Brain Res 169:199-207.
640
641 Dong H, Keegan JM, Hong E, Gallardo C, Montalvo-Ortiz J, Wang B, Rice KC,
642 Csernansky J (2018) Corticotrophin releasing factor receptor 1 antagonists prevent
643 chronic stress-indcued behavioral changes and synapse loss in aged rats.
644 Psychoneuroendocrinology 90:92-101.
645
646 Dong HW, Petrovich GD, Swanson LW (2001) Topography of projections from
647 amygdala to bed nuclei of the stria terminalis. Brain Res Brain Res Rev 38:192-246.
648
649 Dumont EC, Martina M, Samson RD, Drolet G, Pare D (2002) Physiological properties
650 of central amygdala neurons: species differences. Eur J Neurosci 15:545-552.
651
652 Dunlp BW, Binder EB, Iosifescu D, Mathew SJ, Neylan TC, Pape JC, Carrillo-Roa T,
653 Green C, Kinkead B, Grigoriadis D, Rothbaum BO, Nemeroff CB, Mayberg HS (2017)
654 Corticotropin-releasing factor receptor 1 antagonism is ineffective for women with
655 posttraumatic stress disorder. Biol Psychiatry 82(12):866-874.
656
657 Ehrlich I, Humeau Y, Grenier F, Ciocchi S, Herry C, Luthi A (2009) Amygdala inhibitory
658 circuits and the control of fear memory. Neuron 62:757-771.
659
660 Franklin K, Paxinos G (2008) The Mouse Brain in Stereotaxic Coordinates, 3rd Edition.
661 Academic Press.
662
663 Funk CK, O'Dell LE, Crawford EF, Koob GF (2006) Corticotropin-releasing factor within
664 the central nucleus of the amygdala mediates enhanced ethanol self-administration in
665 withdrawn, ethanol-dependent rats. J Neurosci 26:11324-11332.
666
667 Funk CK, Zorrilla EP, Lee MJ, Rice KC, Koob GF (2007) Corticotropin-releasing factor 1
668 antagonists selectively reduce ethanol self-administration in ethanol-dependent rats.
669 Biol Psychiatry 61:78-86.
670
671 Gilpin NW, Herman MA, Roberto M (2015) The central amygdala as an integrative hub
672 for anxiety and alcohol use disorders. Biol Psychiatry 77:859-869.
673

674 Haubensak W, Kunwar PS, Cai H, Ciocchi S, Wall NR, Ponnusamy R, Biag J, Dong
675 HW, Deisseroth K, Callaway EM, Fanselow MS, Luthi A, Anderson DJ (2010) Genetic
676 dissection of an amygdala microcircuit that gates conditioned fear. Nature 468:270-276.
677
678 Heilig M, Godman D, Berrettini W, O'Brien CP (2011) Pharmacogenetic approaches to
679 the treatment of alcohol addiction. Nat Rev Neuroscience 12(11):670-684.
680
681 Herman MA, Contet C, Justice NJ, Vale W, Roberto M (2013) Novel subunit-specific
682 tonic GABA currents and differential effects of ethanol in the central amygdala of CRF
683 receptor-1 reporter mice. J Neurosci 33:3284-3298.
684
685 Herman MA, Contet C, and Roberto M (2016) A functional switch in tonic GABA
686 currents alters the output of central amygdala CRF receptor-1 neurons following chronic
687 ethanol exposure. J Neurosci 36(42):10729-1074.
688
689 Herms J, Dorostkar MM (2016) Dendritic Spine Pathology in Neurodegenerative
690 Diseases. Annu Rev Pathol 11:221-250.
691
692 Herry C, Ciocchi S, Senn V, Demmou L, Muller C, Luthi A (2008) Switching on and off
693 fear by distinct neuronal circuits. Nature 454:600-606.
694
695 Iemolo A, Blasio A, St Cyr SA, Jiang F, Rice KC, Sabino V, Cottone P (2013) CRF-
696 CRF1 receptor system in the central and basolateral nuclei of the amygdala
697 differentially mediates excessive eating of palatable food. Neuropsychopharmacology
698 38:2456-2466.
699
700 Ji G, Fu Y, Adwanikar H, Neugebauer V (2013) Non-pain-related CRF1 activation in the
701 amygdala facilitates synaptic transmission and pain responses. Mol Pain 9:2.
702
703 Justice NJ, Yuan ZF, Sawchenko PE, Vale W (2008) Type 1 corticotropin-releasing
704 factor receptor expression reported in BAC transgenic mice: implications for reconciling
705 ligand-receptor mismatch in the central corticotropin-releasing factor system. J Comp
706 Neurol 511:479-496.
707
708 Kehne JH, Cain CK (2010) Therapeutic utility of non-peptidic CRF1 receptor
709 antagonists in anxiety, depression, and stress-related disorders: evidence from animal
710 models. Pharmacol Ther 128(3):460-487
711
712 Kemppainen S, Pitkanen A (2000) Distribution of parvalbumin, calretinin, and calbindin-
713 D(28k) immunoreactivity in the rat amygdaloid complex and colocalization with gamma-
714 aminobutyric acid. J Comp Neurol 426:441-467.
715
716 Kim J, Zhang X, Muralidhar S, LeBlanc SA, Tonegawa S (2017) Basolateral to Central
717 Amygdala Neural Circuits for Appetitive Behaviors. Neuron 93:1464-1479 e1465.
718

719 Koob GF (2003) Neuroadaptive mechanisms of addiction: studies on the extended
720 amygdala. Eur Neuropsychopharmacol 13:442-452.
721
722 Koob GF (2008) A role for brain stress systems in addiction. Neuron 59:11-34.
723
724 Koob GF (2010) The role of CRF and CRF-related peptides in the dark side of
725 addiction. Brain Res 1314:3-14.
726
727 Li H, Penzo MA, Taniguchi H, Kopec CD, Huang ZJ, Li B (2013) Experience-dependent
728 modification of a central amygdala fear circuit. Nat Neurosci 16:332-339.
729
730 Lin S, Boey D, Lee N, Schwarzer C, Sainsbury A, Herzog H (2006) Distribution of
731 prodynorphin mRNA and its interaction with the NPY system in the mouse brain.
732 Neuropeptides 40:115-123.
733
734 Loughlin SE, Islas MI, Cheng MY, Lee AG, Villegier AS, Leslie FM (2006) Nicotine
735 modulation of stress-related peptide neurons. J Comp Neurol 497:575-588.
736
737 Lowery-Gionta EG, Navarro M, Li C, Pleil KE, Rinker JA, Cox BR, Sprow GM, Kash TL,
738 Thiele TE (2012) Corticotropin releasing factor signaling in the central amygdala is
739 recruited during binge-like ethanol consumption in C57BL/6J mice. J Neurosci 32:3405-
740 3413.
741
742 Marchant NJ, Densmore VS, Osborne PB (2007) Coexpression of prodynorphin and
743 corticotrophin-releasing hormone in the rat central amygdala: evidence of two distinct
744 endogenous opioid systems in the lateral division. J Comp Neurol 504:702-715.
745
746 McCullough KM, Morrison FG, Hartmann J, Carlezon WA, Ressler KJ (2018) Quantified
747 Coexpression Analysis of Central Amygdala Subpopulations. eNeuro 5.
748
749 McDonald AJ (1982) Neurons of the lateral and basolateral amygdaloid nuclei: a Golgi
750 study in the rat. J Comp Neurol 212:293-312.
751
752 McGuire JL, Larke LE, Sallee FR, Herman JP, Sah R (2011) Differential Regulation of
753 Neuropeptide Y in the Amygdala and Prefrontal Cortex during Recovery from Chronic
754 Variable Stress. Front Behav Neurosci 5:54.
755
756 Menzaghi F, Rassnick S, Heinrichs S, Baldwin H, Pich EM, Weiss F, Koob GF (1994)
757 The role of corticotropin-releasing factor in the anxiogenic effects of ethanol withdrawal.
758 Ann N Y Acad Sci 739:176-184.
759
760 Merchenthaler I, Maderdrut JL, Cianchetta P, Shughrue P, Bronstein D (1997) In situ
761 hybridization histochemical localization of prodynorphin messenger RNA in the central
762 nervous system of the rat. J Comp Neurol 384:211-232.
763

764 Mulholland PJ, Chandler LJ (2007) The thorny side of addiction: adaptive plasticity and
765 dendritic spines. ScientificWorldJournal 7:9-21.
766
767 Nie Z, Schweitzer P, Roberts AJ, Madamba SG, Moore SD, Siggins GR (2004) Ethanol
768 augments GABAergic transmission in the central amygdala via CRF1 receptors.
769 Science 303:1512-1514.
770
771 Nielsen DM (2014) Corticotropin-releasing factor type-1 receptor antagonists: the next
772 class of antidepressants?. Life Sci 78(9):909-919
773
774 Paretkar T, Dimitrov E (2019) Activation of enkephalinergic (Enk) interneurons in the
775 central amygdala (CeA) buffers the behavioral effects of persistent pain. Neurobiol Dis
776 124:364-372.
777
778 Penzo MA, Robert V, Li B (2014) Fear conditioning potentiates synaptic transmission
779 onto long-range projection neurons in the lateral subdivision of central amygdala. J
780 Neurosci 34:2432-2437.
781
782 Petrovich GD, Risold PY, Swanson LW (1996) Organization of projections from the
783 basomedial nucleus of the amygdala: a PHAL study in the rat. J Comp Neurol 374:387-
784 420.
785
786 Phillips M, Pozzo-Miller L (2015) Dendritic spine dysgenesis in autism related disorders.
787 Neurosci Lett 601:30-40.
788
789 Pitkanen A, Amaral DG (1994) The distribution of GABAergic cells, fibers, and terminals
790 in the monkey amygdaloid complex: an immunohistochemical and in situ hybridization
791 study. J Neurosci 14:2200-2224.
792
793 Pomrenze MB, Fetterly TL, Winder DG, Messing RO (2017) The corticotropin releasing
794 factor receptor 1 in alcohol use disorder: still a valid drug target?. Alcohol Clin Exp Res
795 41(12):1986-1999
796
797 Poulin JF, Castonguay-Lebel Z, Laforest S, Drolet G (2008) Enkephalin co-expression
798 with classic neurotransmitters in the amygdaloid complex of the rat. J Comp Neurol
799 506:943-959.
800
801 Qiao H, Li MX, Xu C, Chen HB, An SC, Ma XM (2016) Dendritic Spines in Depression:
802 What We Learned from Animal Models. Neural Plast 2016:8056370.
803
804 Roberto M, Cruz MT, Gilpin NW, Sabino V, Schweitzer P, Bajo M, Cottone P, Madamba
805 SG, Stouffer DG, Zorrilla EP, Koob GF, Siggins GR, Parsons LH (2010) Corticotropin
806 releasing factor-induced amygdala gamma-aminobutyric Acid release plays a key role in
807 alcohol dependence. Biol Psychiatry 67:831-839.
808

809 Schindelin J, Arganda-Carreras I, Frise E, Kaynig V, Longair M, Pietzsch T, Preibisch S,
810 Rueden C, Saalfeld S, Schmid B, Tinevez JY, White DJ, Hartenstein V, Eliceiri K,
811 Tomancak P, Cardona A (2012) Fiji: an open-source platform for biological-image
812 analysis. Nat Methods 9:676-682.
813
814 Schwarzer C (2009) 30 years of dynorphins--new insights on their functions in
815 neuropsychiatric diseases. Pharmacol Ther 123:353-370.
816
817 Spiga S, Mulas G, Piras F, Diana M (2014) The "addicted" spine. Front Neuroanat
818 8:110.
819
820 Spierling SR, Zorrilla EP (2017) Don't stress about CRF: assessing the translational
821 failures of CRF1 antagonists. Psychopharmacology 234:1467-1481
822
823 Sun N, Cassell MD (1993) Intrinsic GABAergic neurons in the rat central extended
824 amygdala. J Comp Neurol 330:381-404.
825
826 Sun N, Roberts L, Cassell MD (1991) Rat central amygdaloid nucleus projections to the
827 bed nucleus of the stria terminalis. Brain Res Bull 27:651-662.
828
829 R Core Team RC (2018) R: A language and environment for statistical computing.
830 Foundation for Statistical Computing, Vienna, Austria.
831
832 Tye KM, Prakash R, Kim SY, Fenno LE, Grosenick L, Zarabi H, Thompson KR,
833 Gradinaru V, Ramakrishnan C, Deisseroth K (2011) Amygdala circuitry mediating
834 reversible and bidirectional control of anxiety. Nature 471:358-362.
835
836 Valdez GR, Zorrilla EP, Roberts AJ, Koob GF (2003) Antagonism of corticotropin-
837 releasing factor attenuates the enhanced responsiveness to stress observed during
838 protracted ethanol abstinence. Alcohol 29:55-60.
839
840 Van Pett K, Viau V, Bittencourt JC, Chan RK, Li HY, Arias C, Prins GS, Perrin M, Vale
841 W, Sawchenko PE (2000) Distribution of mRNAs encoding CRF receptors in brain and
842 pituitary of rat and mouse. J Comp Neurol 428:191-212.
843
844 Varodayan FP, Sidhu H, Kreifeldt M, Roberto M, Contet C (2018) Morphological and
845 functional evidence of increased excitatory signaling in the prelimbic cortex during
846 ethanol withdrawal. Neuropharmacology 133:470-480.
847
848 Veinante P, Freund-Mercier MJ (1998) Intrinsic and extrinsic connections of the rat
849 central extended amygdala: an in vivo electrophysiological study of the central
850 amygdaloid nucleus. Brain Res 794:188-198.
851
852 Veinante P, Stoeckel ME, Freund-Mercier MJ (1997) GABA- and peptide-
853 immunoreactivities co-localize in the rat central extended amygdala. Neuroreport 8:
854 2985-2989.

Veinante P, Stoeckel ME, Lasbennes F, Freund-Mercier MJ (2003) c-Fos and peptide immunoreactivities in the central extended amygdala of morphine-dependent rats after naloxone-precipitated withdrawal. Eur J Neurosci 18:1295-1305.

Wiedenmayer CP, Noailles PA, Angulo JA, Barr GA (2002) Stress-induced preproenkephalin mRNA expression in the amygdala changes during early ontogeny in the rat. Neuroscience 114:7-11.

Yu K, Garcia da Silva P, Albeanu DF, Li B (2016) Central Amygdala Somatostatin Neurons Gate Passive and Active Defensive Behaviors. J Neurosci 36:6488-6496.

Zorrilla EP, Koob GF (2004) The therapeutic potential of CRF1 antagonists for anxiety. Expert Opin Investig Drugs 13(7):799-828

869 **Figure Legends**

870 **Figure 1. Calcium binding protein expression in CRF_1+ cells in the CeA.**
871 Representative images of double immunostaining for GFP and **A.** parvalbumin (PV=red,
872 GFP=green), **B.**, calretinin (CR=red, GFP=green), and **C-D.** calbindin (CB=red,
873 GFP=green) in the CeA of CRF_1:GFP mice. Co-expression patterns are visualized in
874 overlaid images in the third column where the arrowhead indicates a single-labeled
875 GFP+ cell, the open arrow indicates a single-labeled CB+ cell, and filled arrows indicate
876 double-labeled cells that co-express GFP and CB (**A-C,** scale=50 μm; **D**, scale=20 μm).
877 **E**. Summary bar graph representing the total number of CBP+ cells counted in the CeA.
878 **F**. Bar graph representing the proportion of CRF_1+ cells co-expressing each CBP. **G**.
879 Bar graph representing the proportion of CBP+ cells co-expressing CRF_1. Data are
880 shown as mean ± SEM. Figure Contributions: HS performed experiments and analyzed
881 data.

882

883 **Figure 2**. **Co-expression of *Gad2* or *Slc17a7* RNA in *Crhr1*+ nuclei.**
884 **A.** Schematic of CeA, with CeL and CeM indicated, is overlaid on tiled image of the CeA
885 in which *Crh* (green), *Crhr1* (red), and DAPI (blue) are shown. Image acquisition
886 position of the CeA (approximately bregma -1.46mm) is shown on Nissl stained image
887 (Franklin and Paxinos mouse brain atlas compact third edition) to indicate the region of
888 interest. **B.** Representative images indicate the co-expression of GFP and *Crhr1* in the
889 GFP:CRF_1 mice in CeL (58% n=8 images) and CeM (86% n=7 images) (*Crhr1*=red,
890 *GFP*=green, DAPI=blue; scale=10 μm). **C**. *Crhr1* probe specificity was validated in the
891 septum of wild type mice, a region of low *Crhr1*/GFP expression (n=2 images).

892 Negligible expression was observed in the septum as compared to the infralimbic
893 prefrontal cortex in the same slice (*Crhr1*=red, DAPI=blue; scale=10μm). **D.**
894 Representative images for *Gad2* (upper; green=*Gad2*, red=*Crhr1*, blue=DAPI; n=5
895 images) and *Slc17a7* (lower; green=*Slc17a7*, red=*Crhr1*, blue=DAPI; n=7 images) in the
896 CeL (scale=10 μm). **E**. Heat map represents the percent of nuclei expressing (from left
897 to right) RNA of interest, *Crhr1,* and co-expression in the total nuclei counted in the CeL.
898 **F**. Heat map represents the percent of nuclei co-expressing in the *Crhr1*+ population of
899 nuclei in the CeL. Color scale from 100% (yellow) to 0% (purple). **G.** Representative
900 images for *Gad2* (upper; green=*Gad2*, red=*Crhr1*, blue=DAPI; n=5 images) and
901 *Slc17a7* (lower; green=*Slc17a7*, red=*Crhr1*, blue=DAPI; n=7 images) in the CeM
902 (scale=10 μm). **H**. Heat map represents the percent of nuclei expressing (from left to
903 right) RNA of interest, *Crhr1*, and co-expression in the total nuclei counted in the CeM. **I**.
904 Heat map represents the percent of nuclei co-expressing in the *Crhr1*+ population of
905 nuclei in the CeM. Color scale from 100% (yellow) to 0% (purple). Data are shown as
906 mean ± SEM. **J.** Representative negative control images for the bacterial probe *DapB* in
907 the CeM indicate negligible fluorescence intensity for both channels shown (*DapB*=red,
908 *DapB*=green, DAPI=blue; scale=10 μm). Figure Contributions: SW and SD performed
909 experiments and SW analyzed data.
910
911 **Figure 3. Co-expression of RNA of interest in *Crhr1*+ nuclei in the CeL**.
912 Representative images from top to bottom for **A.** *Penk* (green=*Penk*, red=*Crhr1*,
913 blue=DAPI; n=8 images), **B.** *Sst* (green=*Sst*, red=*Crhr1*, blue=DAPI; n=9 images), **C.**
914 *Pdyn* (green=*Pdyn*, red=*Crhr1*, blue=DAPI; n=10 images), **D.** *Prkcd* (green=*Prkcd*,

red=*Crhr1*, blue=DAPI; n=9 images), **E.** *Crh* (green=*Crh*, red=*Crhr1*, blue=DAPI; n=10 images), and **F.** *Npy* (green=*Npy*, red=*Crhr1*, blue=DAPI; n=9 images) in the CeL (scale=10 μm). **G**. Heat map represents the percent of nuclei expressing (from left to right) RNA of interest, *Crhr1*, and co-expression in the total nuclei counted in the CeM. **H**. Heat map represents the percent of nuclei co-expressing in the *Crhr1*+ population of nuclei in the CeM. Color scale from 100% (yellow) to 0% (purple). **I.** Quantification of the difference between the percent nuclei expressing RNA of interest (*Crh*, *Prkcd*, *Pdyn*, *Npy*, *Penk*, and *Sst*) in *Crhr1*+ nuclei versus *Crhr1*- nuclei in the CeL (mean ± SEM). Figure Contributions: SW performed experiments and analyzed data.

Figure 4. Co-expression of RNA of interest in *Crhr1*+ nuclei in the CeM. Representative images from top to bottom for **A**. *Penk* (green=*Penk*, red= *Crhr1*, blue=DAPI; n=11 images), **B**. *Sst* (green=*Sst*, red=*Crhr1*, blue=DAPI; n=10 images), **C.** *Crh* (green=*Crh*, red=*Crhr1*, blue=DAPI; n=11 images), **D.** *Pdyn* (green=*Pdyn*, red=*Crhr1*, blue=DAPI; n=8 images), **E.** *Prkcd* (green=*Prkcd*, red=*Crhr1*, blue=DAPI; n=6 images), and **F.** *Npy* (green=*Npy*, red=*Crhr1*, blue=DAPI; n=8 images) in the CeM. **G**. Heat map represents the percent of nuclei expressing (from left to right) RNA of interest, *Crhr1*, and co-expression in the total nuclei counted in the CeM. **H**. Heat map represents the percent of nuclei co-expressing in the *Crhr1*+ population of nuclei in the CeM. Color scale from 60% (yellow) to 0% (purple). **I** Quantification of the difference between the percent nuclei expressing RNA of interest (*Crh*, *Prkcd*, *Pdyn*, *Npy*, *Penk* ($p=0.004$), and *Sst*) in *Crhr1*+ nuclei versus *Crhr1*- nuclei in the CeM (mean ± SEM; **, $p<0.01$ unpaired t-test). **J** Bar graph showing the difference in log2 of the signal intensity

between CeL and CeM of *Crhr1* (n=3079 nuclei), *Npy* (n=90 nuclei), *Penk* (n=468 nuclei), *Crh* (n=273 nuclei), *Prkcd* (n=276 nuclei), Pdyn (n=141 nuclei), and *Sst* (n=145 nuclei) in *Crhr1*+ nuclei (mean ± SEM; ***, p<0.001 unpaired t-test from CeL). Figure Contributions: SW performed experiments and analyzed data.

Figure 5. Spine density and morphology of CRF_1+ and CRF_1- neurons in the CeA. Representative images of dendritic segments in **A.** CRF_1+ and **B.** CRF_1- neurons from the CeM of CRF_1:GFP male mice (scale=10 μm). **C.** Summary bar graph indicates spine density in CRF_1+ and CRF_1- neurons averaged over 10 μm dendritic segments (*, p<0.05 paired t-test). **D.** Summary graph indicates proportion of mushroom spines, stubby spines, thin spines and filopodia in CRF_1+ and CRF_1- neurons in the CeA. (*, p<0.05, paired t-test). Data are shown as mean ± SEM (n=4 mice). Figure Contributions: HS performed experiments and HS and CC analyzed data.

Figure 6. Membrane properties and glutamatergic transmission of CRF_1+ and CRF_1-neurons in the CeA. A. Representative current-clamp recordings from three cell-types: regular spiking (left), low threshold bursting (middle) and late spiking (right) from a CeA neuron. **B.** Distribution of cell-types recorded from for CRF_1- (n=15) and CRF_1+ (n=16) CeA neurons. **C.** Representative traces of mEPSCs in CRF_1+ (top) and CRF_1- (bottom) CeA neurons. **D and E.** Frequency and amplitude of mEPSCs in CRF_1+ (n=16) and CRF_1- (n=12) CeA neurons. **F.** Representative traces of sEPSCs in CRF_1+ (top) and CRF_1- (bottom) CeA neurons. **G and H.** Frequency and amplitude of sEPSCs in CRF_1+ (n=14) and CRF_1- (n=14) CeA neurons. **I.** Representative traces of mEPCS

during baseline (top) and 200 nM CRF application (bottom) from CRF_1+ CeA neurons. **J and K.** CRF effects on frequency and amplitude of mEPSCs in CRF_1+ (n=11) and CRF_1- (n=9) CeA neurons, respectively. **L.** Average trace of mEPSC during baseline (black) and 200nM CRF (green) application from a CRF_1+ CeA neuron. **M and N.** CRF effects on rise and decay time of mEPSCs in CRF_1+ and CRF_1- CeA neurons, respectively. (*, $p < 0.05$ by one-sample t-test). Data are shown as mean ± SEM. Figure Contributions: RP performed experiments and analyzed data.

Table Legends

Table 1. Membrane properties of recorded CeA neurons.

The membrane capacitance, resistance, time constant and resting potential are reported for CRF_1+ and CRF_1- neurons recorded from the CeA. Data are shown as mean ± SEM. Contributions: RP performed experiments and analyzed data.

Table 2. Summary of mEPSC and sEPSC characteristics.

The frequency, amplitude, rise time, and decay time of mEPSCs and sEPSCs are reported for CRF_1+ and CRF_1- neurons recorded from the CeA. Data are shown as mean ± SEM. Contributions: RP performed experiments and analyzed data.

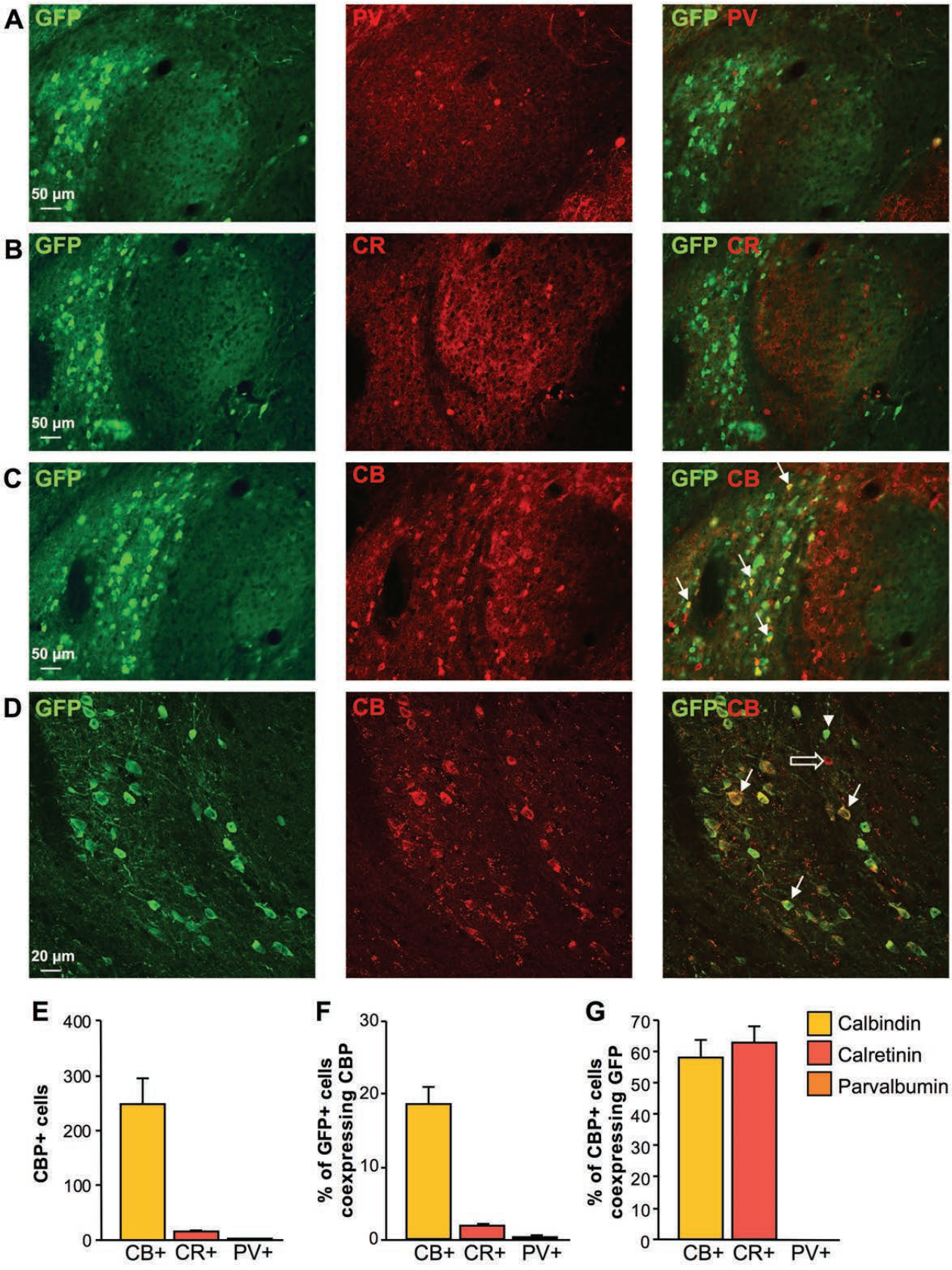

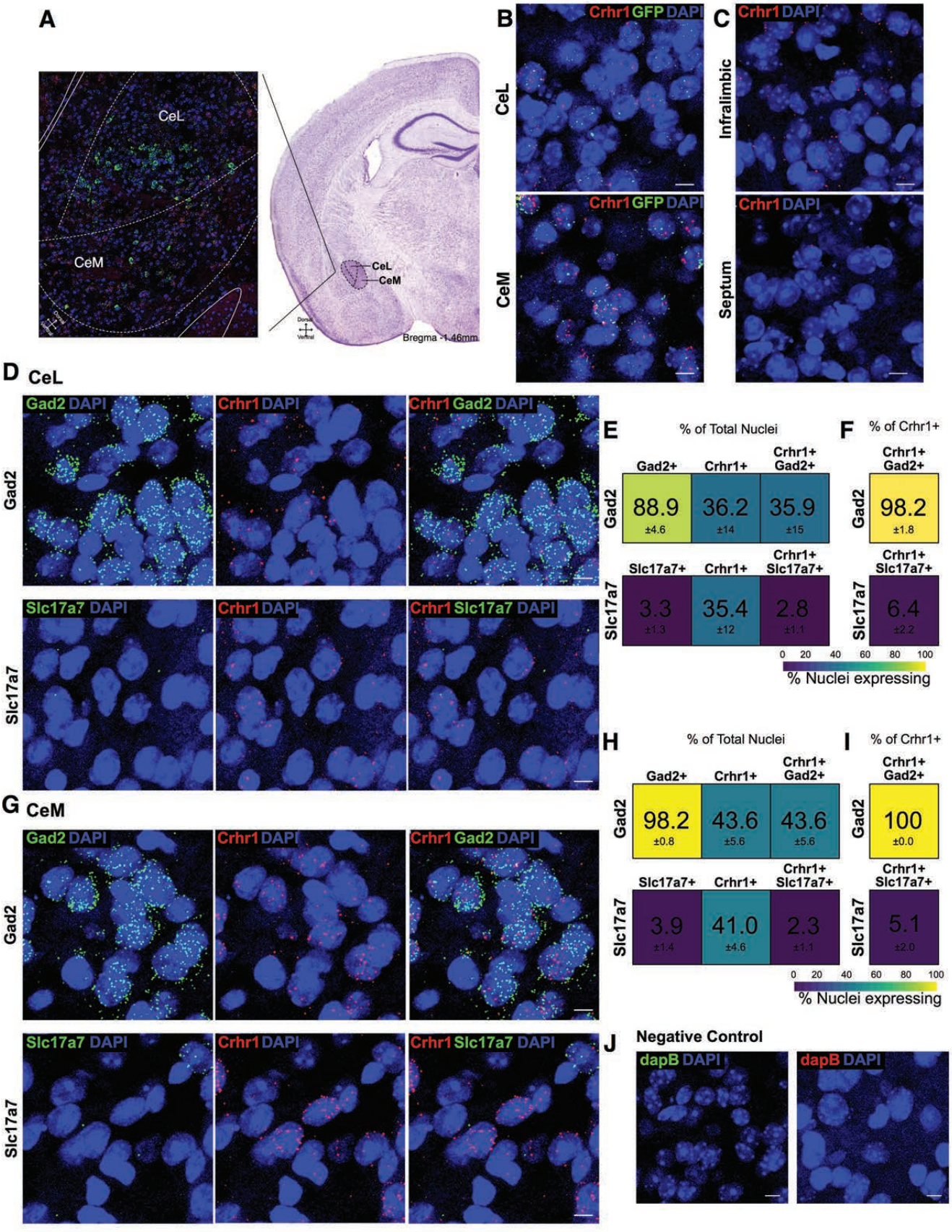

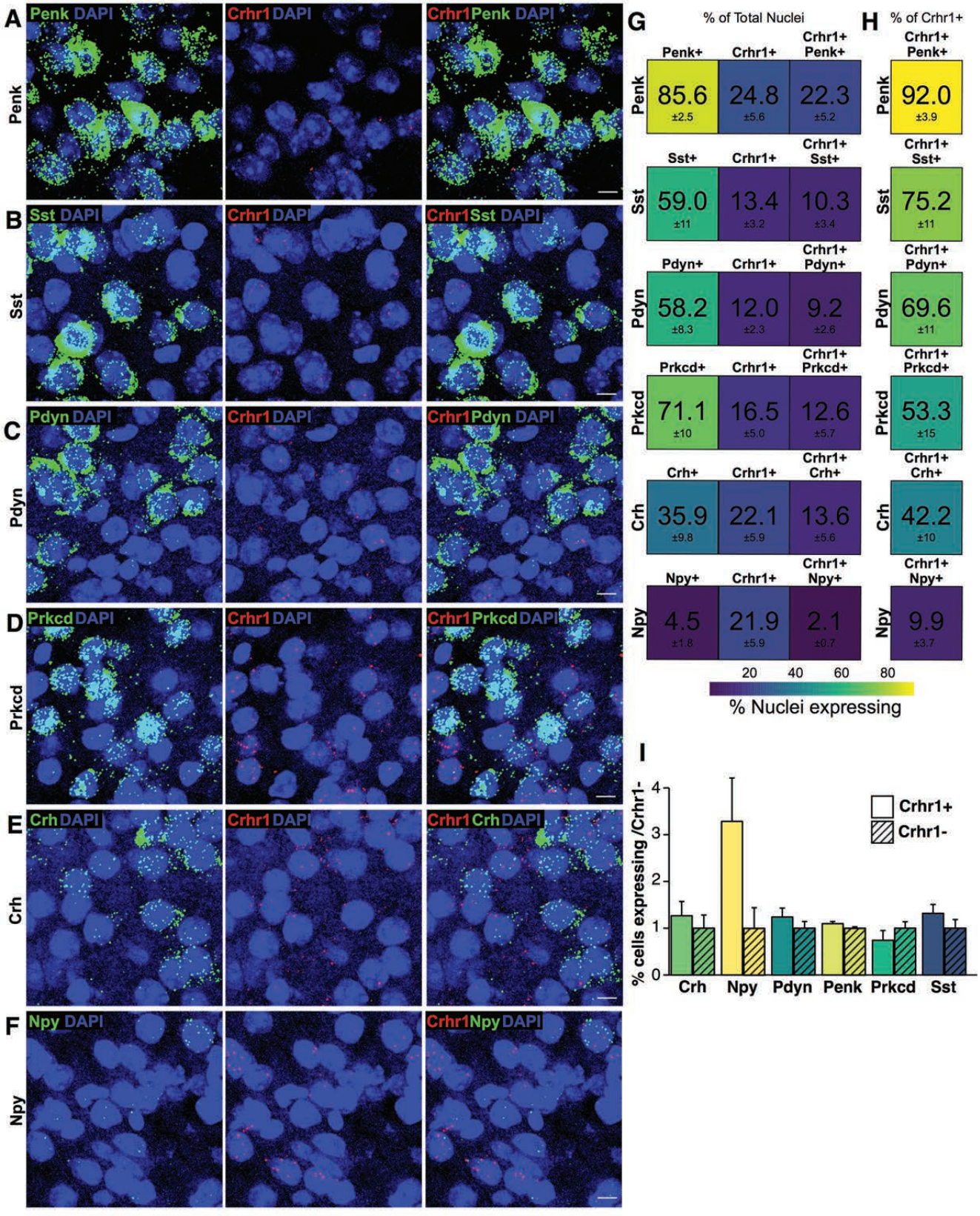

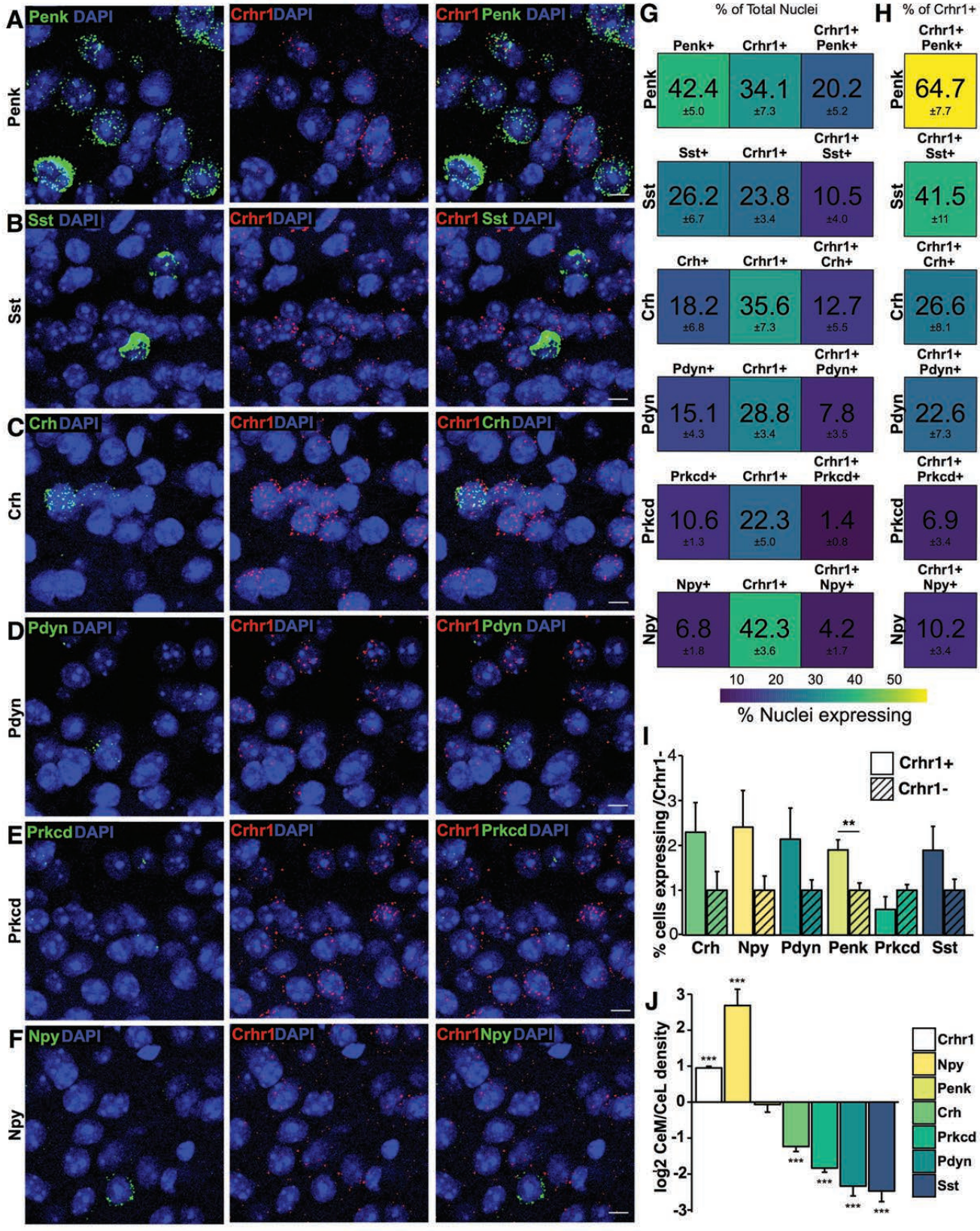

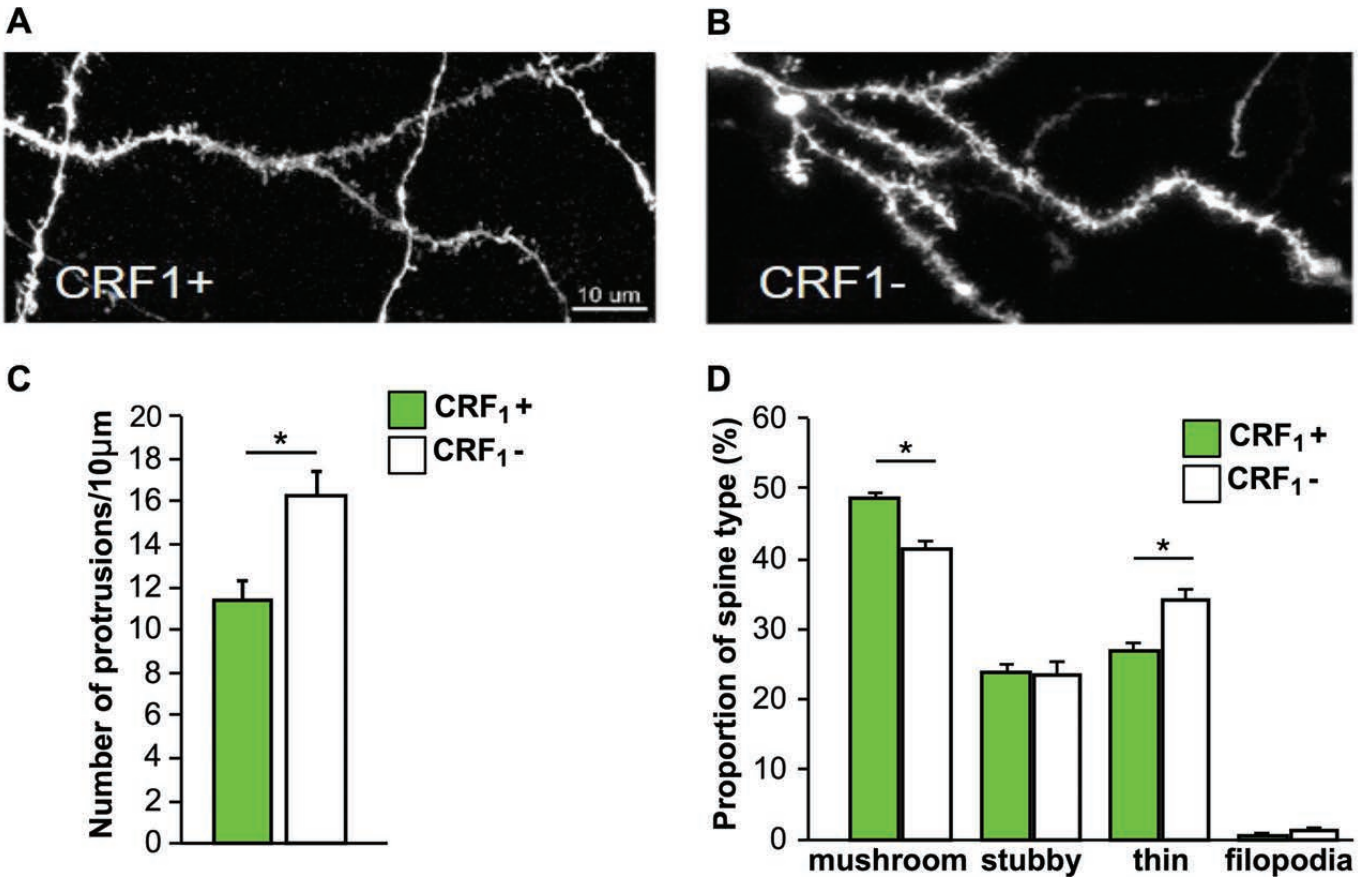

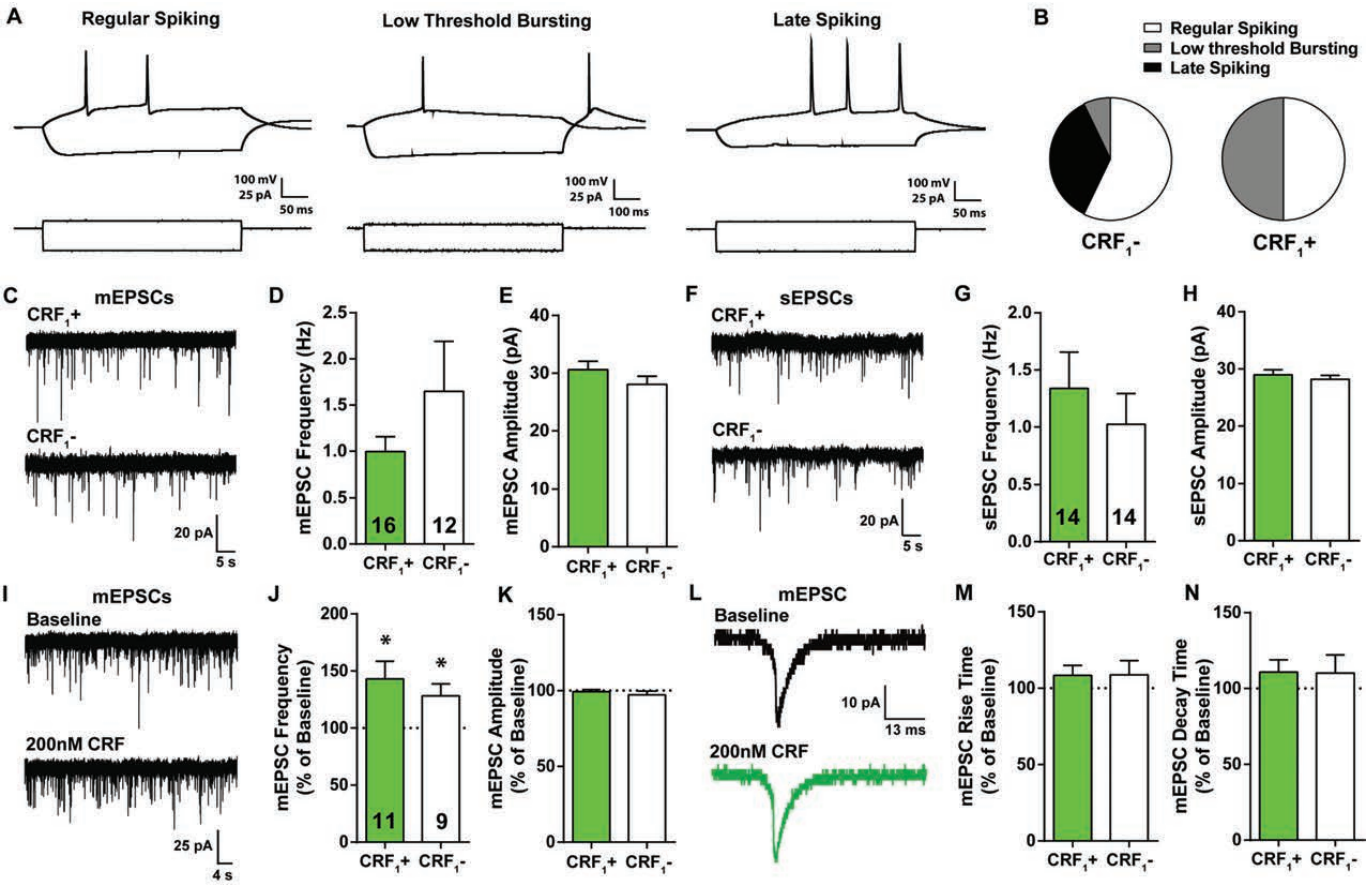

Table 1 . Membrane properties of recorded CeA neurons. The membrane capacitance, resistance, time constant and resting potential are reported for CRF1+ and CRF1- neurons recorded from the CeA. Data are shown as mean ± SEM. Contributions: RP performed experiments and analyzed data.

	Membrane Capacitance (pF)	*Membrane Resistance (MΩ)*	*Time Constant (ms)*	*Resting Membrane Potential (mV)*
CRF_1+	44.36 ± 2.7	476.0 ± 34.8	369.2 ± 52.4	-52.1 ± 1.8
CRF_1-	49.91 ± 2.9	456.2 ± 13.3	348.4 ± 55.5	-52.6 ± 1.8

Table 2. Summary of mEPSC and sEPSC characteristics. The frequency, amplitude, rise time, and decay time of mEPSCs and sEPSCs are reported for CRF1+ and CRF1- neurons recorded from the CeA. Data are shown as mean ± SEM. Contributions: RP performed experiments and analyzed data.

		Frequency (Hz)	Amplitude (pA)	Rise Time (msec)	Decay Time (msec)
mEPSCs					
	CRF_1-	1.64 ± 0.54	28.09 ± 1.40	0.95 ± 0.14	0.56 ± 0.10
	CRF_1+	0.99 ± 0.16	30.63 ± 1.43	1.02 ± 0.06	0.56 ± 0.06
sEPSCs					
	CRF_1-	1.02 ± 0.26	28.18 ± 0.68	0.84 ± 0.07	0.60 ± 0.07
	CRF_1+	1.33 ± 0.31	28.96 ± 0.87	0.90 ± 0.10	0.62 ± 0.08